Characterization of a New Anti-Cancer Compound Using Multi-Cellular Tumour Spheroids

Kevin Larocque

A
Thesis
in the Department
of
Biology

Presented in Partial Fulfillment of the Requirements
For the Degree of
Master of Science (Biology) at
Concordia University
Montreal, Quebec, Canada

August 2018

CONCORDIA UNIVERSITY
School of Graduate Studies

This is to certify that the thesis prepared

By: Kevin Larocque

Entitled: Characterization of a Novel Anti-Cancer Compound Using Multi-Cellular Tumor Spheroids

and submitted in partial fulfillment of the requirements for the degree of

Master of Science (Biology)

complies with the regulations of the University and meets the accepted standards with respect to originality and quality.

Signed by the final Examining Committee:

Patrick Gulick Chair
Dr. Patrick Gulick

Madoka Gray-Mitsumune External Examiner
Dr. Madoka Gray-Mitsumune

David Kwan Examiner
Dr. David Kwan

Malcolm Whiteway Examiner
Dr. Malcolm Whiteway

Alisa Piekny Supervisor
Dr. Alisa Piekny

Approved by Robert Weladji
Dr. Robert Weladji, Graduate Program Director

Fall 2018 Patrick Gulick

Dean of Faculty

Abstract

Kevin Larocque

We synthesized a thieonoisoquinoline scaffold amenable to modifications and found that several derivatives selectively kill cancer cells in the nanomolar range. Further characterization of one of these molecules, C75, revealed that it uniquely targets spindle poles. This phenotype is due to specific functional groups and not the scaffold because another derivative, C87, has no effect on cells. To demonstrate C75's potential for use *in vivo*, we found that C75 successfully regresses or inhibits the growth of multi-cellular tumour spheroids grown from HeLa (cervical cancer), A549 (lung cancer) and HCT-116 (colorectal cancer) cells. Since C75 is a small molecule, we also determined if controlling its delivery and release would improve its efficacy in spheroids. As a proof-of-concept, we tested the release of Doxorubicin (Dox) from novel polymer-based nanoparticles with dual-controlled release in HeLa and A549 spheroids. Dox levels from nanoparticles increased sooner, and to a greater extent within the core of spheroids vs. free Dox. Encapsulating C75 in similar nanoparticles increased its efficacy in HeLa and A549 spheroids compared to free compound. Lastly, we also explored the potential to use C75 in combination therapies with paclitaxel (Taxol^{TM}), which is an anti-cancer drug that patients often develop resistance to and/or causes severe side-effects. We found that C75 and paclitaxel have different mechanisms of action at a cellular level, and cause regression of HCT 116 spheroids when used in combination at subthreshold doses. Thus, our results show that C75 has the potential to be explored for its use as an anti-cancer drug.

Acknowledgements

I would like to thank Dr. Piekny for giving me the opportunity to do research on a project that I loved and in mentoring me through the process.

Also, I would like to thank my committee members, Dr. David Kwan and Dr. Malcolm Whiteway for their advice and guidance.

In addition, I would like to thank Héloïse Vuong and Sylvie Ouellette for their help and time. Moreover, I would to thank all my labmates: Daniel Beaudet, Karina Mastronardi, Dilan Jaunky, Imge Özügergin, Nhat Pham, Mathieu Husser and Brandon Jaunky.

Finally, I liked to thank the CMCI, specifically Dr. Chris Law and Dr. Chloë van Ostende Triplet for helping me in taking and analysing images.

Dedications

I would like to dedicate my thesis to my parents, Daniel Larocque and Nathalie Pellerin for teaching me the value of hard work and for supporting me in my studies. Making you proud is the greatest reward. Also, to my girlfriend Mélissa McAuley, who has supported me through late nights and early mornings, I love you.

Contribution of Authors

Figure 4A. Jiang Tian Liu and Fei Chen synthesized the compounds shown.

Figures 4B and C. Dilan Jaunky performed the experiments shown.

Figure 5. Dilan Jaunky performed the experiments shown.

Figure 8A. Sung Hwa Hong designed the nanoparticles shown.

Figure 10. Sung Hwa Hong performed the experiments shown.

Table of Contents

List of Figures

Abbreviations

ACA anti-centromere antibody

CAM Cell adhesion molecules

DAPI 4′,6-diamidino-2-phenylindole

Dox Doxorubicin

HSET/KIFC1 kinesin like protein 1

ILK integrin linked kinase

MAPs microtubule associated proteins

MDR Multi-drug resistance

NPs nanoparticles

GTP Gaunosine triphosphate

ROS Reactive oxygen species

γ-Turc Gamma tubulin ring complex

Spheroids Multi-cellular tumour spheroids

FDA Fluorescein diacetate

PI Propidium iodide

THF Tetrahydrofuran

PCM Pericentriolar material

Ch-TOG Colonic and hepatic Tumor overexpressed gene.

Portions of this thesis were taken from the following manuscripts:

1. Hong, S.H., **Larocque, K.**, Jaunky, D., Piekny, A., and Oh, J. (2018). Dual disassembly and biological evaluation of enzyme/oxidation-responsive polyester-based nanoparticulates for tumor-targeted delivery. *Colloids and Surfaces B: Biointerfaces*. Submitted.

2. Jaunky, B. D*., **Larocque, K*.**, Husser, C, M., Hong, H. S., Liu, T. J., Chen, F., Oh, K.J., Forgoine, P., and Piekny, A. (2018). A novel compound that selectively disrupts spindle pole integrity in cancer cells. *Scientific Reports*. Submitted.

1. Introduction

My thesis describes the effect of a novel anti-cancer compound, C75, on cancer cells grown as multi-cellular tumour spheroids. In the current era of personalized medicine, treatments are being tailored to more precisely match tumour genotypes to give patients the best chance of survival. However, this approach is limited by the number of available cancer drugs. In addition, due to the overuse of current therapies, a common challenge is the development of resistance. Thus, there is a need to develop alternative drugs that can be used in place of, or in combination with existing therapies. Dr. Pat Forgione's lab (Chemistry, Concordia University) synthesized C75 and we found that it functions as a spindle inhibitor that selectively kills cancer cells in the nanomolar range. To determine its potential for *in vivo* use, I characterized its efficacy on spheroids grown from different cancers. This included optimizing its delivery in collaboration with Dr. John Oh's lab (Chemistry, Concordia University) and testing the ability to use C75 in combination with a commonly used chemotherapeutic drug.

Cancer remains one of the leading causes of death in Canada, yet few new treatments have entered the market in the last decade. Approximately 200,000 Canadians were diagnosed with cancer in the past year, and this number is projected to rise as the proportion of seniors in our population increases (Canadian Cancer Society). Cancer is a complex disease that is difficult to treat due to the multiple hallmarks that they acquire which help them adapt to their environment and evolve (Hanahan & Weinberg, 2011). One of these hallmarks is sustained proliferation, which is targeted by some of the most successful chemotherapeutic drugs (Hanahan & Weinberg, 2011). However, many of these drugs can cause severe side effects and/or patients can develop resistance, leaving them with few alternatives (Cao et al., 2017). Some are no longer used as first-line

treatments due to their harsh side effects such as Doxorubicin (Dox), which is an anthracycline cytotoxic drug that arrests cells in S phase (McGowan et al., 2017). It binds to DNA and topoisomerase II causing double stranded break, inhibiting DNA replication (McGowan et al., 2017). However, one of the advantages of performing studies with Dox is that it has intrinsic fluorescent properties that can be used to track its location inside cells or tissue (Changenet-Barret et al., 2013). With some drugs being taken off the market, and few entering, there is a need to develop new treatments to expand the repertoire of available drugs.

1.1 Paclitaxel as a Microtubule Stabilizer

Paclitaxel (Taxol^{TM}) is an effective anti-cancer drug because it functions as a spindle inhibitor that disrupts microtubule dynamics causing mitotic arrest. Microtubules and microtubule associated proteins (MAPS) are required to build mitotic spindles. Microtubules are composed of 13 protofilaments, each consisting of α and β tubulin dimers that bind to GTP (Lüders and Stearns, 2007). In cells, nucleation often occurs at the γ-Turc complexes, which are found at the centrosome (Figure 1; Lüders and Stearns, 2007; Tilney et al., 1973). Microtubules have dynamic instability, which is determined by the state of GTP hydrolysis. This property of growing and shrinking is essential to form a functional bipolar spindle and for proper kinetochore attachment to chromosomes (Lüders and Stearns, 2007). Paclitaxel disrupts microtubule dynamics by binding to beta tubulin on the inside surface of microtubules (Dumontet and Jordan., 2010). This causes their stabilization and increases the rate of polymerization (Dumontet and Jordan., 2010). Since cancer cells proliferate more rapidly in comparison to healthy cells, paclitaxel and other cell cycle inhibitors tend to show selectivity for cancer cells *in vitro* and *in vivo*. In addition, machineries that govern the mitotic spindle tend to be altered due to the over or under-expression of key regulators, making them more sensitive to disruption. For example, aurora A kinase regulates the spindle poles for mitotic spindle assembly by phosphorylating and regulating complexes such as TACC3 and ch-TOG, which loads onto the minus ends of microtubules and regulates microtubule polymerization (Burgess et al., 2015). Thus, the dynamics of microtubules may be altered in some cancer cells and more easily perturbed by even low levels of microtubule-targeting drugs. However, many of the small molecule compounds currently used as anti-cancer drugs suffer from stability and solubility issues *in vivo*, requiring frequent administration of large doses intravenously. Thus, healthy cells can also be affected causing side-effects. A desirable approach

is to find a high-quality drug with a molecular target or process that is uniquely altered in cancer vs. healthy cells.

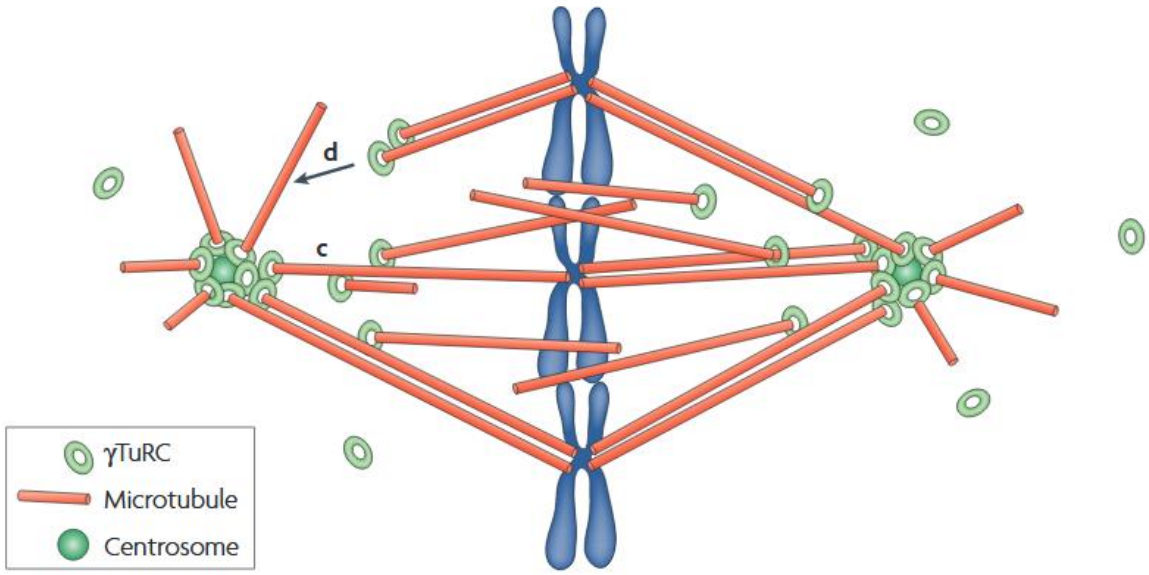

Figure 1: Mitotic spindle in somatic animal cells. A cartoon schematic shows the bipolar spindle, built from two centrosomes positioned at opposite poles of the cell. The γTurc complex assembles at the centrosomes and templates the nucleation of microtubules that align chromosomes in the equatorial plane. Image taken from Lüders and Stearns (2007).

Many cancer cells have aberrant centrosomes, either due to amplification or fragmentation and require clustering mechanisms to form bipolar spindles. Centrosomes are the major sites of microtubule nucleation in the cell. In a healthy cell, they duplicate once during S phase and separate during prophase, subsequently giving rise to the spindle (Levine et al., 2017). The amplification or fragmentation of centrosomes is characteristic of multiple cancers from several different tissue types (Levine et al., 2017). Since multipolar spindles lead to drastic changes in ploidy and cell death, cancer cells rely on mechanisms to cluster centrosomes to form bipolar spindles (Figure 2; Levine et al., 2017; Quintyne et al., 2005). One of these mechanisms involves HSET/KIFC1, a minus end directed motor protein that promotes microtubule cross-linking and sliding (Pannu et al., 2015). HSET/KIFC1 knockdown leads to multipolarity and death in cancer cells, however, it is not essential in healthy cells (Pannu et al., 2015). Another mechanism that mediates centrosome clustering involves integrin-linked kinase (ILK). ILK has well-described functions in signal transduction from focal adhesion complexes for cell migration and how it functions in centrosome clustering is not clear (Hannigan et al., 1995; Fielding et al., 2010; Qin and Wu., 2012). However, studies revealed that it may influence the function of the TACC3/ch-TOG complex at the centrosome (Fielding et al., 2010). As with HSET/KIFC1, knockdown or inhibition of ILK causes multipolar spindle phenotypes in cancer cells, but not in healthy cells (Fielding et al., 2010; Pannu et al., 2015). Thus, these proteins could be ideal to target to develop new anti-cancer drugs. However, while inhibitors have been made to HSET/KIFC1 and ILK, they only work at high concentrations and may not suitable for *in vivo* use (Kalra et al., 2009; Watts et al., 2013).

There is a need to develop new, selective, high-quality anti-cancer drugs. A common approach is to perform high throughput screens using indiscriminate libraries to find compounds that inhibit a molecular target of interest (Hay et al., 2014). However, the compounds may not be suitable for *in vivo* use and require complex modifications, which could take years to accomplish and may not be practical for manufacturing at a larger scale. In addition, the target may not be ideal, because it could also be required in a subset of healthy cells. Using a 'blind' approach to screen for phenotypic requirements has been more successful. For example, paclitaxel and some of the other cell cycle inhibitors were discovered by screening extracts from various plants that effectively block cell proliferation and purifying the active compounds (Yun et al., 2012). However, these compounds are difficult to synthesize *in vitro*, and are challenging to modify. Our

novel approach was to synthesize a family of modifiable compounds that already have properties ideal for *in vivo* use, and screen derivatives for phenotypes.

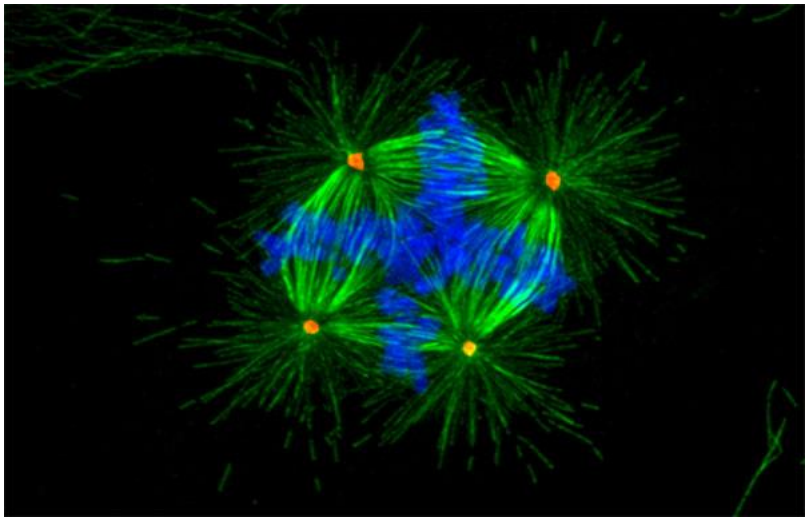

Figure 2: Multipolar spindle phenotype. The cell on the image has multiple spindle poles, four centrosomes and chromosomes ligned in multiple planes. Image from https://www.hhmi.org/bulletin/fall-2014/errors-division, taken by Dr. David Pellman.

1.2 Multi-Cellular Tumor Spheroids

Using spheroids may better predict the efficacy of anti-cancer drugs *in vivo*. Multi-cellular tumour spheroids have multiple characteristics in common with *in vivo* tumors, including some of the problems encountered by small molecule therapies (Friedrich et al., 2009). Spheroids have a proliferating rim at their outer surface, an intermediate zone of quiescent cells and a necrotic core (Sutherland, 1988). These zones reflect the tumour microenvironment formed by the gradients of oxygen and nutrients across the spheroid, which become limiting in the core (Friedrich et al., 2009; Sutherland, 1988). Another interesting feature of spheroids is that once cells are grown in 3D cultures, their gene expression profile changes, many of which are oncogenes that correlate with metastasis, drug resistance, proliferation and other characteristics common in more progressive cancers (Ghosh et al., 2005). For example, the multiple-drug resistance (MDR)1 pump responsible for the efflux of chemotherapeutic drugs from the cell is found to be up-regulated in spheroids over their monolayer counterpart (Oshikata et al., 2011). Other genes mediate cell growth or adhesion. For example, expression of the cell adhesion molecule (CAM) protein mediates cell-cell or cell-matrix interactions to facilitate the spherical organization of the spheroid. CAM's have also been shown to drive tumour invasion and metastasis (Indovina et al., 2008). E-cadherin is another adhesion molecule that is expressed in some spheroids and mediates cell-cell adhesion to form aggregates (Cui et al., 2017). The strength of adhesion junctions is mediated via intracellular catenin complexes and the actin cytoskeleton (Cui et al., 2017). In addition, small molecule drugs also form gradients across spheroids, and could differentially affect cells in different stages of the cell cycle (Phung et al., 2011; Friedrich et al., 2009). Thus, spheroids better predict the efficacy of new anti-cancer drugs in blocking and/or reducing tumours in comparison to cells grown as monolayers (Phung et al., 2011). However, one of the limitations of growing spheroids *in vitro* is that they lack a blood supply and the signals associated with angiogenesis (Friedrich et al., 2009).

1.3 Polymer Based Nanoparticles

Drug efficacy can be improved using a delivery system that targets and/or releases the drug at the site of the tumour *in vivo*. Polymer based nanoparticles (NPs) are biocompatible, physiologically stable, and biodegradable (Van der Ende et al., 2008). Shells with amphipathic properties permit the loading of high concentrations of small compounds and can be designed to release in the presence of stimuli that are typically found at higher levels in cancer cells

(Trachootham et al., 2008; Lorenzo and Concheiro, 2014). The NPs used here are novel and were designed to have dual-controlled release in the presence of reactive oxygen species (ROS) and esterases (Hung et al., submitted). While not selectively targeted per se, their size enriches NPs in the vicinity of tumours as they are retained by the poorly formed vascular network. Here they can enter cells, where in the presence of stimuli, the NPs breakdown and release their cargo in a controlled matter, which should lower their toxicity compared to free drug. As we learn more about lipid profiles and proteins that are uniquely expressed on the surface of cancer cells, this information will guide the improvement of delivery systems to target drugs more selectively.

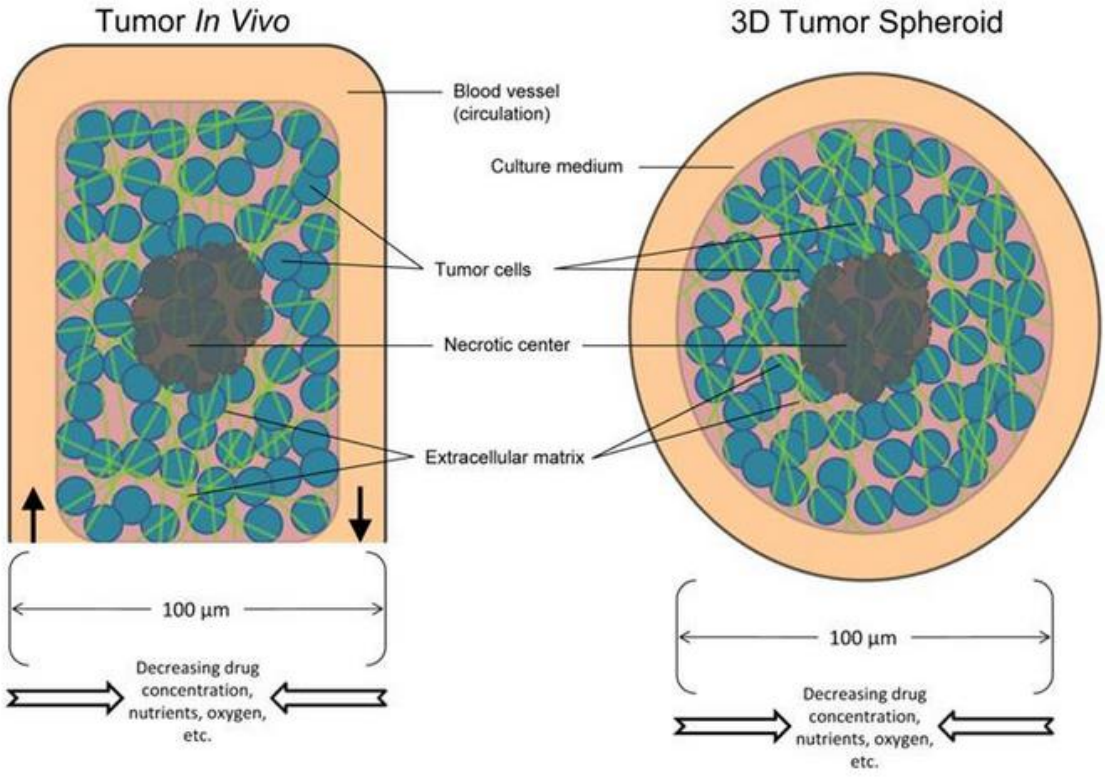

Figure 3: A comparison of tumours in vivo with spheroids. The tumour on the left represents a tumor in a patient. The tumor on the right represents a multi-cellular tumour spheroid. The labeled characteristics are showing differences and similarities between both. Image taken from Phung et al. (2011).

Here, I characterized the efficacy of C75, a new anti-cancer compound, in spheroids. C75 selectively kills cancer cells in the nanomolar range, and I found that C75 effectively disrupts or inhibits spheroids grown from HeLa, A549 and HCT 116 cells. Encapsulating C75 in a novel NP delivery system with dual-controlled release increased its efficacy in spheroids grown from HeLa and A549 cells. Moreover, subthreshold concentrations of C75 and paclitaxel caused regression of HCT 116 spheroids, suggesting that C75 can be explored for its use in combination therapies with commonly used anti-cancer drugs.

2. Methods

2.1 Cell culture

HeLa cells were grown in DMEM (Wisent), while A549 cells were grown in F12K media (Wisent) and HCT 116 (p53-/-) cells were grown in McCoy's media (Wisent) in humidified incubators at 37°C with 5% CO_2. All media were supplemented with 10% fetal bovine serum (FBS; Thermo Scientific), 2 mM L-glutamine (Wisent), 100 U penicillin (Wisent), and 0.1 mg/mL streptomycin (Wisent).

2.2 Drug treatments

C87 and C75 were synthesized by Dr. Forgione's lab and dissolved in dimethyl sulfoxide (DMSO) as 1 mM stocks and kept at -20°C. Working stocks of 100 μM C75 (active derivative) or C87 (inactive derivative) were made using DMSO:H_2O (9:1) before use. Paclitaxel (Bioshop) was dissolved in DMSO as a 10 mM stock and diluted to a range of smaller concentrations before use. Cells grown as single layer cultures (2D) or as spheroids (3D) were treated with varying concentrations of C75, C87 or paclitaxel as indicated. The concentrations of DMSO added to the cells were kept below 0.5%.

2.3 Multi-cellular tumour spheroids

HeLa and HCT 116 spheroids were grown on agarose. Wells of a 96-well dish were coated with 50 μL of 1.5% agarose. Once the agarose was dry, 50 μL of media was added per well. A hemocytometer was used to determine the concentration of cells within the media. Appropriate dilutions were made to obtain a concentration of approximately 500 HeLa or 1000 HCT 116 cells per well. 100 μL of diluted cells were added to each well and the dish was placed in a humidified incubator at 37°C with 5% CO_2 to let the spheroids form and grow. Spheroids were transferred to a 24-well dish after growing to an appropriate size and appearance as monitored via light microscopy, which was approximately 3 days for HeLa spheroids and 5 days for HCT 116 spheroids. Wells in the 24-well dishes were previously coated with 350 μL of 1.5% agarose and 1 mL of media. Drugs were prepared accordingly in a solution of 9:1 DMSO to water, then diluted 1:1 with media before adding it to the wells. Spheroids were collected across a minimum of three independent experiments.

A549 spheroids were grown using the hanging drop method. Cells were counted as described above and drops of media containing 50-100 cells were added to the surface of a lid from a 2 cm cell-culture petri dish. PBS was added to the bottom of the dish to prevent the drops from drying. The lid was then flipped and placed over the bottom of the dish to form hanging drops over the PBS. Dishes were incubated as described above for 3 days. Spheroids were transferred in media to wells of a 24-well dish after growing to an appropriate size and appearance as monitored by light microscopy. Treatments were performed as described above.

Images of spheroids were collected each day at the same time using a Nikon-TIE inverted microscope with the 4x/0.2 (HeLa) or 10x/0.45 (A549 and HCT 116) objectives using the DS-Ri2 ultra high-resolution colour camera (Nikon) and Elements acquisition software (Nikon). HCT 116 spheroids treated with paclitaxel, C75 or both in combination were imaged using the 4x/0.2 objective and the 1.5 magnification changer. Files were opened in Image J for analysis as described below.

Spheroids were stained for live and dead cells using fluorescein diacetate (FDA) and propidium iodide (PI), respectively. FDA (2 µL of 5 mg/mL stock) and PI (10 µL of 2 mg/mL stock) were added directly to the media. PI was added 5 minutes prior to FDA, then the dishes were left for 10 minutes in the dark before imaging using a Nikon-TIE inverted epifluorescence microscope with Lambda XL LED light sources using the objectives as outlined above, a Photometrics Evolve 512 EMCCD camera and Elements acquisition software (Nikon).

2.4 Nanoparticles

To prepare NPs loaded with C75, an organic solution containing 20 mg of synthesized polyester and 1.1 mg of C75 dissolved in 2.5 mL tetrahydrofuran (THF) was mixed with an aqueous solution of 0.2 mg B20 and 20 mg PEG in 10.3 mL of water. The resulting mixture was homogenized using a sonifier (Branson) for 5 minutes (amplitude = 15 %, 10 seconds on, 2.5 seconds off) and stirred for 2 days to remove THF. The solution was then dialyzed in 1 L water (MWCO of dialysis tubing = 12,000 Da) for 6 hours to remove residual THF. The solution was concentrated using a rotary evaporator and filtered through a Polyethersulfone filter with a pore size of 0.45 µm. To determine C75 loading, the extinction coefficient of C75 was determined in a mixture of water/THF (1/4 v/v) using UV/vis spectroscopy. Then, the loading level and the

encapsulation efficiency were determined with mixtures consisting of aliquots of 1 mL C75-loaded NPs mixed with 4 mL of THF. The UV/vis spectra were used to obtain the absorbance of C75 at 320 nm and DLS (Malvern Instruments) was used to determine the size of C75-loaded NPs.

To prepare NPs loaded with Dox, an organic solution containing synthesized polymers (12 mg), Dox (1 mg), and Et_3N (3.5 μL) dissolved in THF (2.8 mL) was mixed with an aqueous solution of B20 (0.6 mg) and PEG (11.5 mg) in water (11.7 mL). The resulting mixtures were homogenized using a sonifier (Branson) for 5 min (amplitude = 15 %, 10 sec on, 2.5 sec off) and stirred for 24 hrs to remove THF. They were then dialyzed over water (1 L) for 6 hrs to remove excess (free) Dox and Et_3N, yielding aqueous Dox-NPs at 2.0 mg/mL. First, the extinction coefficient of Dox was determined in a mixture of water/THF (1/4 v/v) using a UV/vis spectroscopy along with Beer-Lambert equation. Then, the loading level and loading efficiency of Dox were determined with mixtures consisting of aliquots of Dox-NPs (1 mL) mixed with THF (4 mL).

2.5 Immunofluorescence

To monitor mitotic spindle phenotypes, immunofluorescence was performed after various treatments as indicated. Cultured cells were plated on pre-washed and acid-treated coverslips at a confluency of 40-50% and left overnight to adhere. Cells were fixed for immunofluorescence using freshly prepared ice-cold 10% w/v cold trichloroacetic acid for 14 minutes at 4°C. Cells were washed 3-4 times with PBST (PBS with 0.3% Triton X-100) and kept at 4°C prior to staining. After blocking for 20 minutes in 5% normal donkey serum (NDS) in PBST, fixed cells were immunostained for microtubules using 1:400 mouse anti-α-tubulin antibodies (DM1A; Sigma-Aldrich). After washing, anti-mouse Alexa 488 secondary antibodies were used at a 1:500 dilutions in PBST with 5% NDS for 2 hours at room temperature. After washing, 4′,6-Diamidino-2′-phenylindole dihydrochloride (DAPI; Sigma-Aldrich) was added at a 1:1000 dilution (from a 1 mg/mL stock) in PBS for 5 minutes. Cells were then washed with PBST, followed by a wash with 0.1 M Tris pH 9, then drops of mounting media (0.5% propyl gallate in 50% glycerol) were added to the coverslips, which were then mounted onto slides and sealed.

2.6 Microscopy

Fixed slides were imaged using the Nikon-TIE inverted epifluorescence microscope with

Lambda XL LED light sources, using the 60x/1.4 oil objective, a Piezo Z stage (ASI), a Photometrics Evolve 512 EMCCD camera and Elements acquisition software (Nikon). Exposures were kept constant based on controls. Images were acquired as 1 μm Z-stacks and image files were exported as TIFFs, which were opened with Image J (NIH) and converted into maximum intensity Z-stack projections. Projections and merged colour images were then converted into 8-bit images and imported into Illustrator (Adobe) to make figures.

2.7 Analysis

To measure the change in area of the spheroids, image files were exported as TIFFs and analyzed using a macro written for Image J (FIJI; NIH). Images containing a spheroid were passed through "IsoData" thresholding and 10 iterations of the “close” function to fill in pixel size gaps. Spheroids were identified using the “analysis of particles” command in Image J and the area was measured by the software. For spheroids where the integrity was disrupted, the macro was modified to calculate the area. First images were converted to a black background and masked. Then, the “max inscribed circle” function was used to fit a perfect circle to the remaining spheroid structure. The function gives a radius from which the area was calculated.

To analyze the proportion of spindle phenotypes of cells after treatment with C75, paclitaxel, or in combination, Z-stack projections of images were visualized using the NIS-Element software to view cells in three dimensions. Mitotic cells were identified based on condensed DNA stained with DAPI, and were classified as monopolar, bipolar or multipolar based on the number of poles/centrosome fragments observed from the α-tubulin staining. At least 30 individual cells were counted per slide, and experiments were done in triplicate for each treatment to statistically determine the proportion of phenotypes.

The distances between spindle fragments caused by C75 and paclitaxel were analyzed using a macro written for Image J (FIJI; NIH). Image files were exported as TIFFs and opened in Image J as Z-stack projections of maximum intensity and converted to a binary mask. Using the ROI manager, the macro identified each cell in the DAPI channel, then identified the fragments inside the corresponding cells in the tubulin channel. Each fragment correlated with a point of maximum intensity, and the coordinates for that point were recorded. The distance between two

points was measured using the coordinates of each point, and triangulating the distance based on Pythagorean theorem: A2 + B2= C2, C being the distance between 2 given points.

3. Results

3.1 A thienoisoquinoline compound (C75) shows selectivity and high efficacy for cancer cells

To determine if thienoisoquinoline compounds have anti-cancer properties, 30 derivatives were synthesized with the same scaffold by Dr. Forgione's lab (Chemistry, Concordia University; Chen et al., 2014). From this series of compounds, we found that one derivative (C75) decreased cancer cell viability. C75 was further screened for its cytotoxic effect in several different cancer cell lines including HeLa (cervical cancer), A549 (lung cancer) and HCT 116 (colorectal cancer) as well as a non-cancer cell line (HFF-1; foreskin fibroblast; Fig. 4A). Over three population doubling times all of the cancer cell lines had IC_{50} values for viability of ~400 nM, whereas HFF-1 cells had an IC_{50} value of ~800 nM (Figs 4B, C). This two-fold difference in efficacy for cancer versus non-cancer cells suggests that C75 could target a process unique to cancer cells. Another derivative, C87, shares the same scaffold as C75 but lacks several critical functional groups (Fig. 4A) and had no/little effect on cell viability when added up to 1 μM (Fig. 4C). This suggests that the anti-cancer property of C75 is not a general feature of the scaffold itself.

A

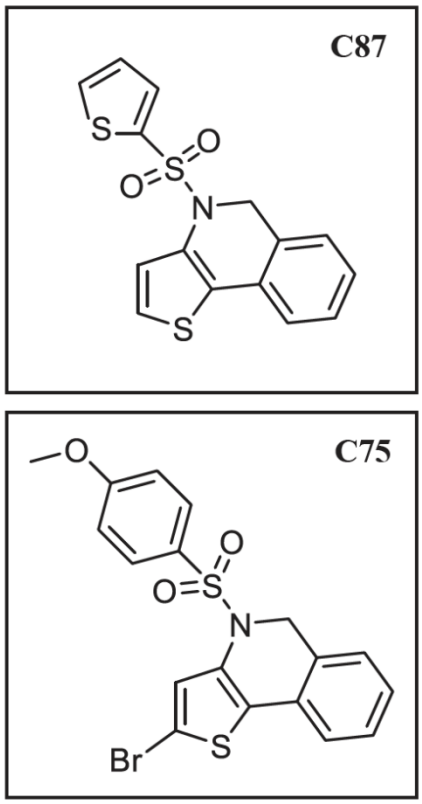

B

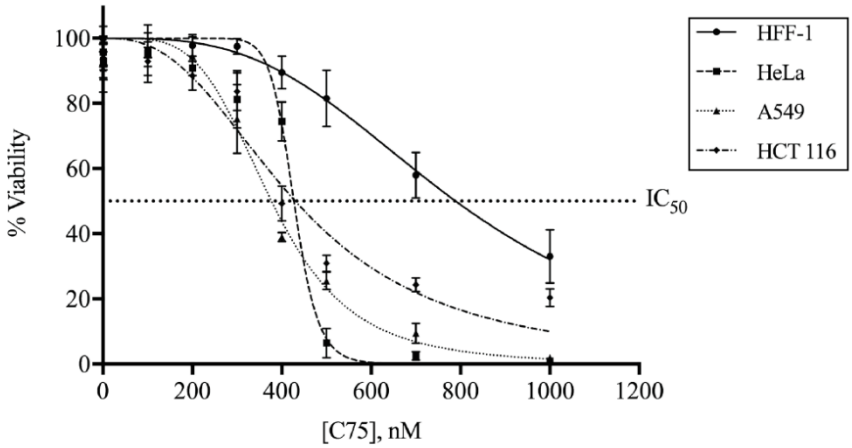

C

	IC_{50}, nM	
Cell Lines	Compound 75	Compound 87
HFF-1	789	> 1000
HeLa	427	> 1000
A549	377	> 1000
HCT 116	431	> 1000

Figure 4: C75 is a thienoisoquinoline compound that selectively decreases cancer cell viability. A) The chemical structures of compound 87 (C87) and 75 (C75) are shown. B) A line graph shows changes in the percentage of viable HFF-1, HeLa, A549 and HCT 116 cells after treatment with a range of C75 concentrations for 3 population doubling times as indicated (N=3). The inhibitory concentration reducing viability of 50% of the population (IC_{50}) is shown by the dotted line. C) A table shows the calculated IC_{50} values for each cell line for C75 and C87 treatments. Jiang Tian Liu and Fei Chen synthesized the compounds shown in A. The data shown in B and C were collected and analyzed by Dilan Jaunky.

3.2 C75 causes cells to arrest in mitosis

To ascertain why C75 reduces cancer cell viability, we determined how it affects the cell cycle. HeLa, A549 or HCT 116 cells were treated with increasing concentrations of C75 for 8 hours, then fixed, permeabilized and stained with propidium iodide (PI) to measure their DNA content by flow cytometry. All three cell lines showed an increase in the proportion of mitotic (G2/M) cells with increasing concentrations of C75, which was more obvious when the data was plotted as line graphs (Fig. 5A). A Tukey's multiple comparison test revealed that there was a significant increase in the proportion of mitotic HeLa and A549 cells treated with 300 – 400 nM of C75, which continued to increase at 500 nM. This occurred at the expense of cells in G0/G1, which decreased over the same concentrations. However, HCT 116 cells responded to C75 at lower concentrations of C75. There was an significant increase in the proportion of G2/M cells treated with 100 – 200 nM of C75 that continued to increase up to 500 nM. While this increase corresponded with a decrease in the G0/G1 population, the proportion of cells in S phase also started to decrease between 400 – 500 nM of C75.

Mitotic arrest is typically caused by spindle phenotypes due to unattached kinetochores and/or decreased inter-centromere tension, which fails to satisfy the spindle assembly checkpoint (Akhmanova and Steinmetz, 2015). To determine if C75 causes mitotic spindle phenotypes, HeLa, A549 and HCT 116 cells were fixed and stained for chromatin with DAPI (in blue), tubulin to visualize microtubules (in green) and ACA to stain centromeres (site of kinetochore attachments; in red) after 8 hours of C75-treatment. In all three cell types, we observed aberrant mitotic spindles, with misaligned chromosomes and fragmented spindle poles at higher concentrations of C75 (Fig. 5B).

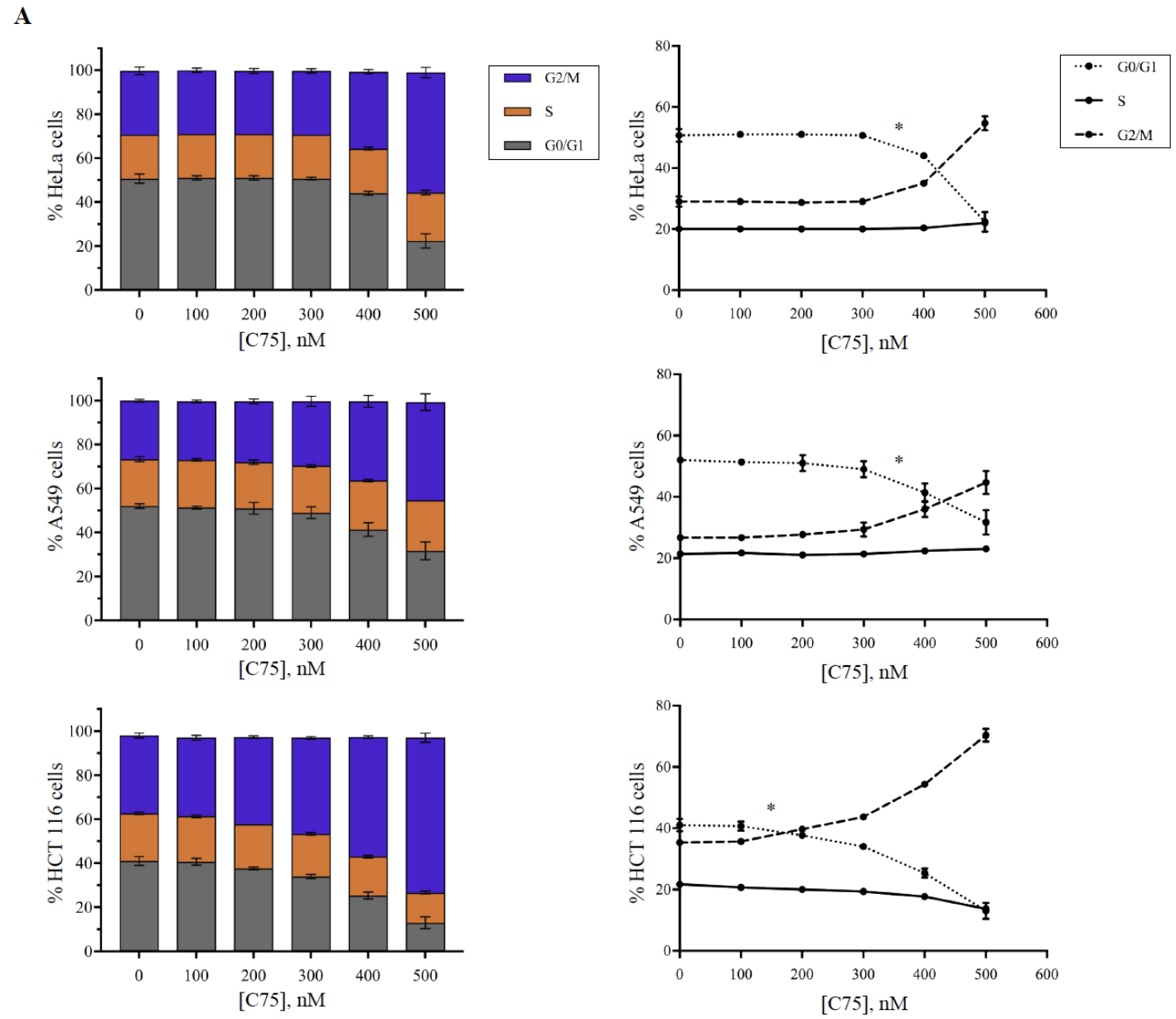
A
% HeLa cells
% A549 cells
% HCT 116 cells
[C75], nM
G2/M
S
G0/G1
*
B
HeLa
A549
HCT 116
DAPI/
Tubulin/ACA
Control
300 nM C75
500 nM C75

Figure 5: C75 causes cells to arrest in mitosis. A) Bar graphs (left) illustrate changes in the proportion of HeLa, A549 and HCT 116 cells in different phases of the cell cycle after treatment with a range of C75 concentrations for 8 hours determined by flow cytometry. For each condition, 20,000 cells were counted per replicate (N=3). Line graphs (right) highlight the relative changes in the cell cycle for the different treatments. The bars for all graphs show standard deviation. B) Immunofluorescence images show HeLa, A549 and HCT 116 cells co-stained for DAPI (chromatin; blue), tubulin (microtubules; green) and ACA (kinetochores; red) 8 hours after treatment with C87 or 300 or 500 nM C75. The scale bar is 10 μm. The asterisks indicate statistical significance of $p<0.05$ using the Tukey's multiple comparison test. The data in A and B were collected and analyzed by Dilan Jaunky.

3.3 C75 disrupts or regresses spheroids grown from cancer cell lines

Our data shows that C75 reduces cancer cell viability in the nanomolar range. To determine if it similarly affects cancer cells grown in more complex environments, C75 was added to cells that were induced to form multi-cellular tumour spheroids. As described in the introduction, spheroids are composed of many cells that form unique interactions in 3D. As spheroids grow, they develop three major regions; an outer proliferative rim, a quiescent zone and an inner necrotic core due to limiting gradients of nutrients and oxygen (Sutherland, 1988). Since spheroids contain cells in different states of proliferation and have different microenvironments, they may better predict the efficacy of anti-cancer drugs *in vivo* (Friedrich et al., 2009; Hirschhaeuser et al., 2010; Patel et al., 2015; Stadler et al., 2015). Spheroids grown from HeLa cells were completely disrupted within two days of treatment with 500 nM of C75, but not with 250 nM C75 or 1 μM C87 (control; Fig. 6A). Spheroids grown from A549 or HCT 116 cells failed to grow or significantly decreased in size when treated with 500 nM or 1 μM of C75, but not 1 μM C87 (control; Figs 6B, C). Staining spheroids for live cells using fluorescein diacetate (FDA) or dead cells using PI revealed that control spheroids for all of the cell lines contained mostly live cells with dead cells in the necrotic core (Fig. 7). The majority of cells in C75-treated HeLa spheroids were dead by day 2 (Fig. 7). A549 spheroids treated with C75 lost their integrity and shed large pools of dead cells, while HCT 116 spheroids progressively decreased in size, but retained live cells (Fig. 6). These data suggest that C75 successfully disrupts or causes regression of spheroids from different cell lines at concentrations that are still within nanomolar range (*e.g.* < 1 μM), although each cell line shows unique responses. Thus, C75 retains high efficacy in reducing cancer cell viability when cells are grown in more complex environments.

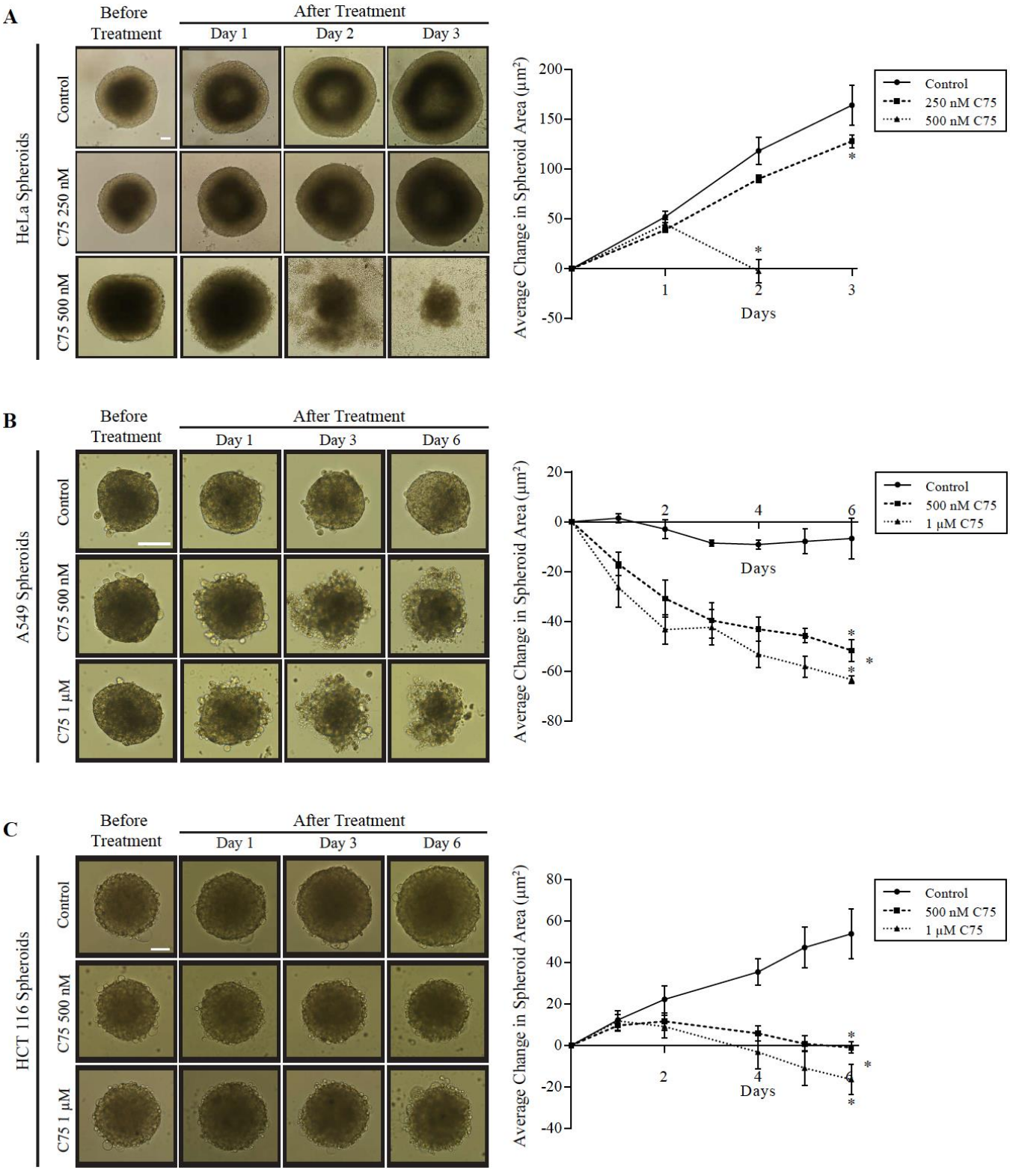
A
Before Treatment
After Treatment
Day 1
Day 2
Day 3
HeLa Spheroids
Control
C75 250 nM
C75 500 nM
Average Change in Spheroid Area (µm²)
Days
Control
250 nM C75
500 nM C75
B
Before Treatment
After Treatment
Day 1
Day 3
Day 6
A549 Spheroids
Control
C75 500 nM
C75 1 µM
Average Change in Spheroid Area (µm²)
Days
Control
500 nM C75
1 µM C75
C
Before Treatment
After Treatment
Day 1
Day 3
Day 6
HCT 116 Spheroids
Control
C75 500 nM
C75 1 µM
Average Change in Spheroid Area (µm²)
Days
Control
500 nM C75
1 µM C75

Figure 6: C75 disrupts or regresses spheroids grown from multiple cell lines. A) Brightfield images show HeLa spheroids over 3 days before and after treatment with control C87, 250 nM or 500 nM C75 (n=10 for each treatment). A line graph to the right shows the change in spheroid area (μm^2) for each day and treatment as indicated. B) A549 spheroids and a line graph are shown as in A), except that 500 nM and 1 μM C75 (n=6 for each treatment) were used, and spheroids were monitored over a longer period of time (6 days). C) HCT 116 spheroids and a line graph are shown as in B) (n=10 for each treatment). The scale bar for all images is 0.1 mm. Bars on all graphs show standard deviation. The asterisks indicate $p<0.05$ using the student t test.

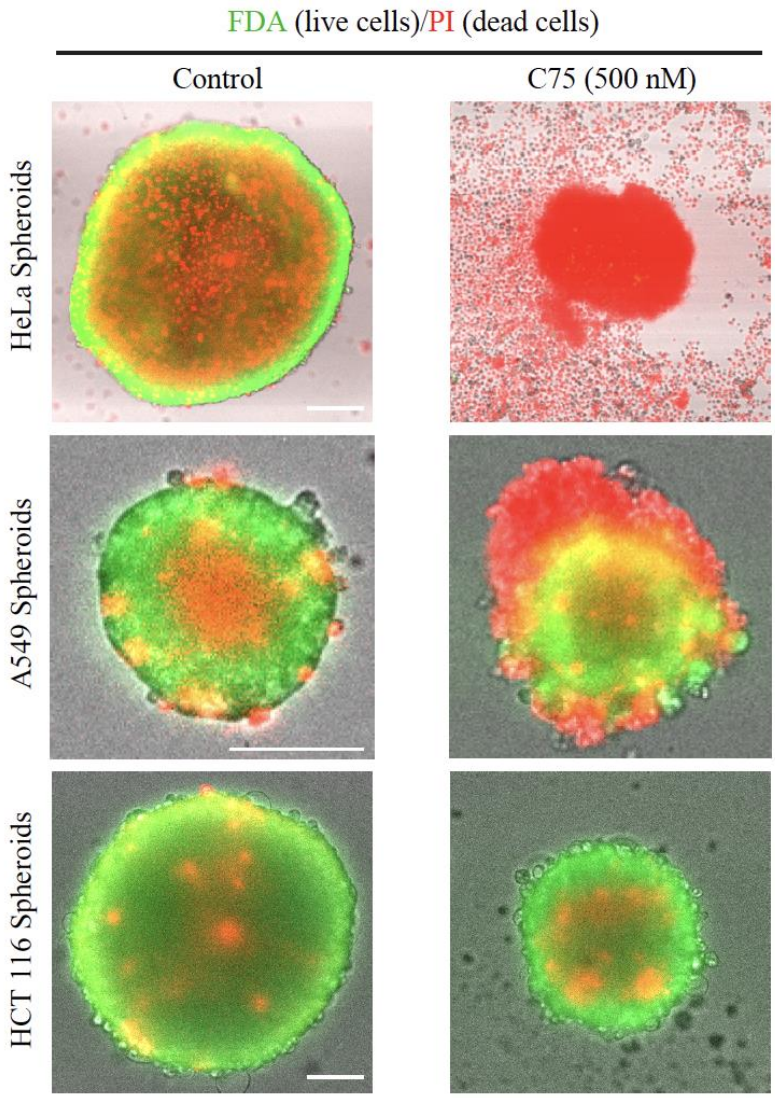

Figure 7: C75 increases the proportion of dead cells and shrinks the proportion of live cells in spheroids. Images show HeLa, A549 and HCT 116 spheroids co-stained with fluorescein diacetate (FDA; green) to visualize live cells and propidium iodide (PI; red) to visualize dead cells after treatment with control (1 µM C87) or 500 nM C75. The scale bar for all images is 0.1 mm. Images are taken at the last day of treatment, 3 days for HeLa and 6 days for HCT 116 and A549.

3.4 Nanoparticles deliver Doxorubicin to cells in spheroids more efficiently than free drug

NPs can be used as a delivery system for compounds to improve their efficacy and reduce side-effects. Small molecules may form a gradient across spheroids or tumours that reduces their concentration toward the interior. In addition, compounds that block cell proliferation may not be as effective against quiescent cells. A novel NP with dual-controlled release was designed by John Oh's lab (Chemistry, Concordia University; Fig. 8). These NPs have an amphipathic shell that encapsulates compounds and contains cleavage sites for ROS and esterases, which are typically enriched in cancer cells (Fig. 8). While the goal is to use these NPs to deliver C75, we first tested their delivery of Dox, a commonly used anti-cancer drug that can be detected by fluorescence with excitation at 480 nm and emission at 590 nm. HeLa spheroids were incubated with Dox-loaded NPs or free Dox at 1.6 μg/mL, or empty NPs as a control for 4 days. As shown in the images of HeLa spheroids, the fluorescence intensity appeared higher in spheroids treated with NP-loaded vs. free Dox after several days (Fig. 9A). Quantitative analysis of the levels revealed that spheroids treated with NP-loaded Dox had a sharp increase in fluorescence within 6 hrs, which steadily increased with time (Fig. 9B). After 4 days of incubation, the levels were five times greater in spheroids treated with NP-loaded Dox vs. free Dox (Fig. 9C). These results suggest that NPs can more efficiently deliver Dox to the inner regions of HeLa spheroids compared to free drug.

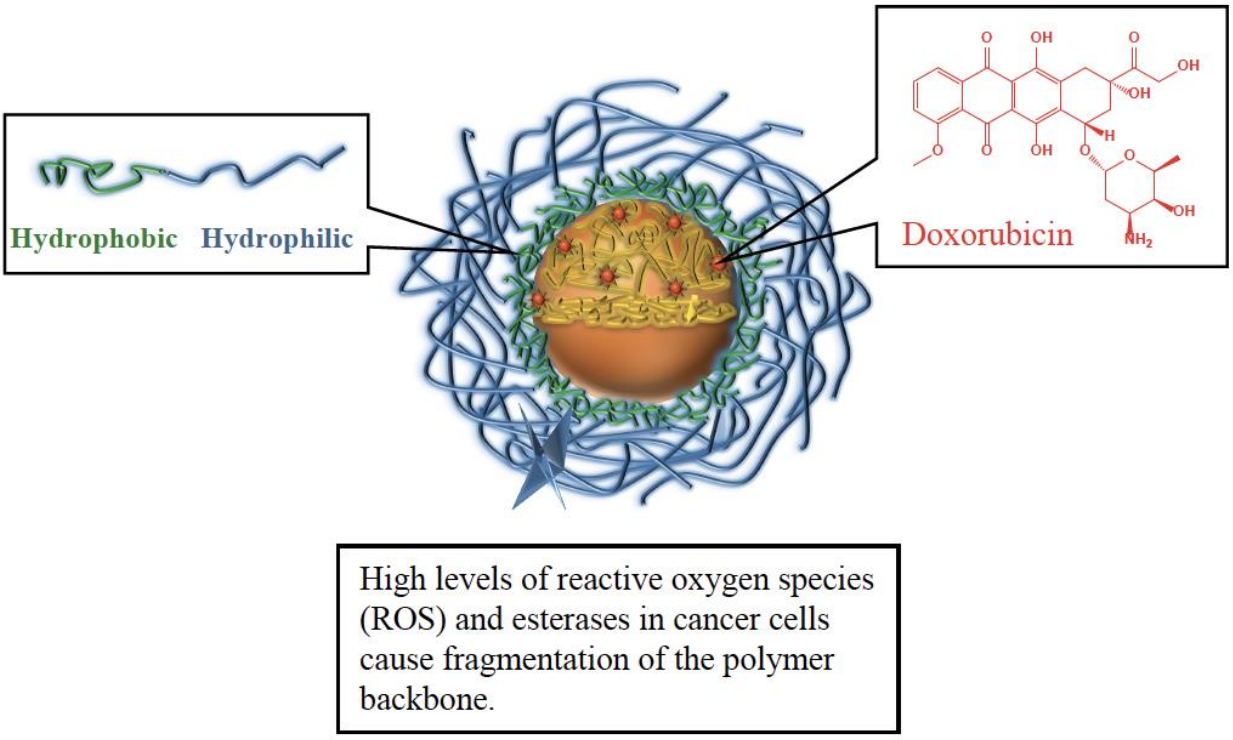

Figure 8: Dual responsive polymer-based nanoparticles. A) A cartoon schematic shows the design of the biodegradable polymeric NPs used in this study. Amphipathic molecules form a hydrophobic, polyester core that interacts with the compound, and a hydrophilic shell that interacts with the surrounding environment. Cleavage sites permit their destabilization in the presence of ROS and esterases. The NPs were designed by Sung Hwa Hong.

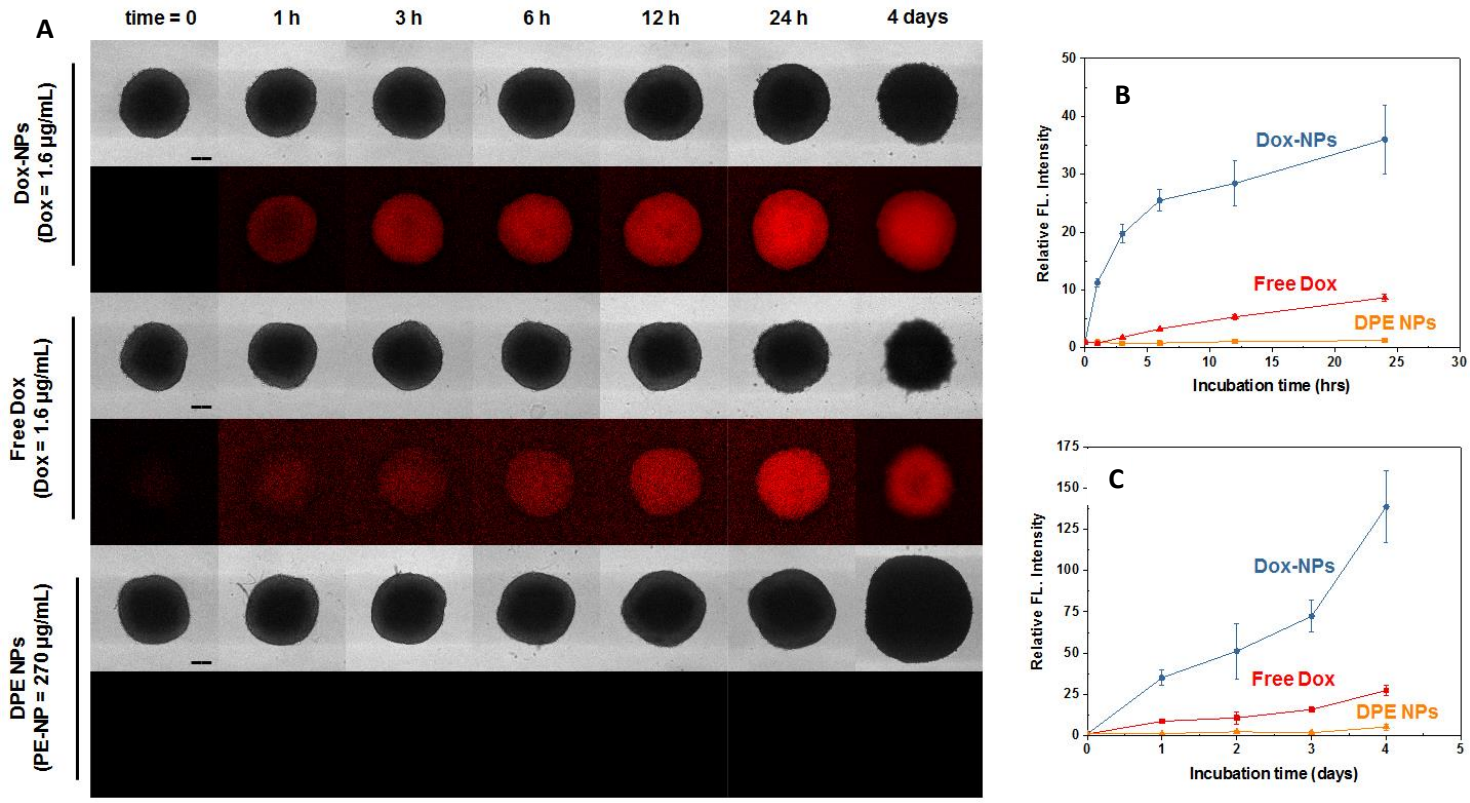

Figure 9: Nanoparticles loaded with Doxorubicin localizes at a higher rate than free drug. A) Fluorescent images show HeLa spheroids treated with NPs loaded with 3 µM Dox for 4 days in comparison to free Dox (middle) or empty NPs (DPE NPs; bottom). *Note that the images were processed differently for free Dox vs. Dox-NPs due to the low signals from free Dox. The scale bar for all images is 0.2 mm. B) Line graphs show the changes in relative fluorescence intensity for spheroids treated with Dox-NPs, free Dox or empty NPs over time in hours or days (n=3 for each treatment) (C). Each value was normalized by their initial value. Bars show standard deviation.

3.5 Nanoparticle delivery of C75 increases its efficacy in spheroids

Next, we determined if encapsulated C75 could more effectively disrupt spheroids in comparison to free drug. C75 was encapsulated in the same NPs described above (Fig. 8). C75 showed a linear correlation with concentration at 320 nm, which was used to calculate the amount of C75 loaded into NPs (Fig. 10). Both HeLa and A549 spheroids showed enhanced response to encapsulated C75. HeLa spheroids were completely disrupted 2 days after treatment with 250 nM of NP-loaded C75, while the integrity of A549 spheroids was completely disrupted 4 days after treatment with 500 nM (Fig. 11). However, HCT 116 spheroids did not show an enhanced response, which could reflect differences in the mechanism of NP uptake and/or the levels of ROS or esterase required to degrade the NPs in the different cell lines (Fig. 11).

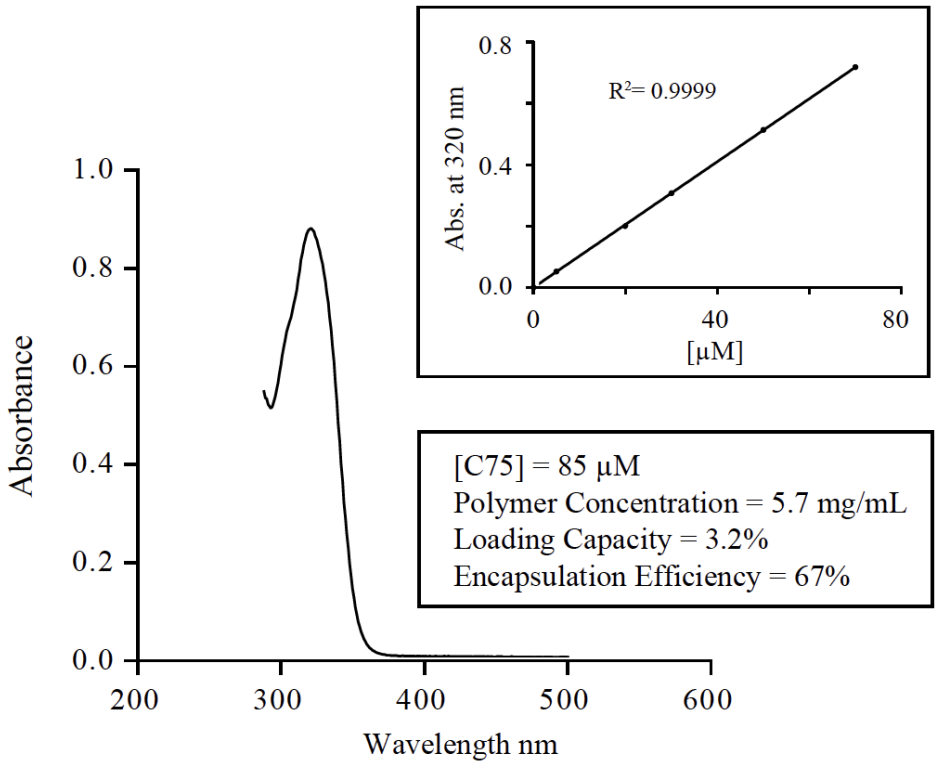

Figure 10: Absorbance of C75 linearly correlates with concentration. A graph (upper right) shows the linear increase in absorbance of C75 at 320 nm with increasing concentration, and the graph underneath and box shows characteristics of C75-loaded NPs determined by peak absorbance at 320 nm. This data was collected by Sung Hwa Hong.

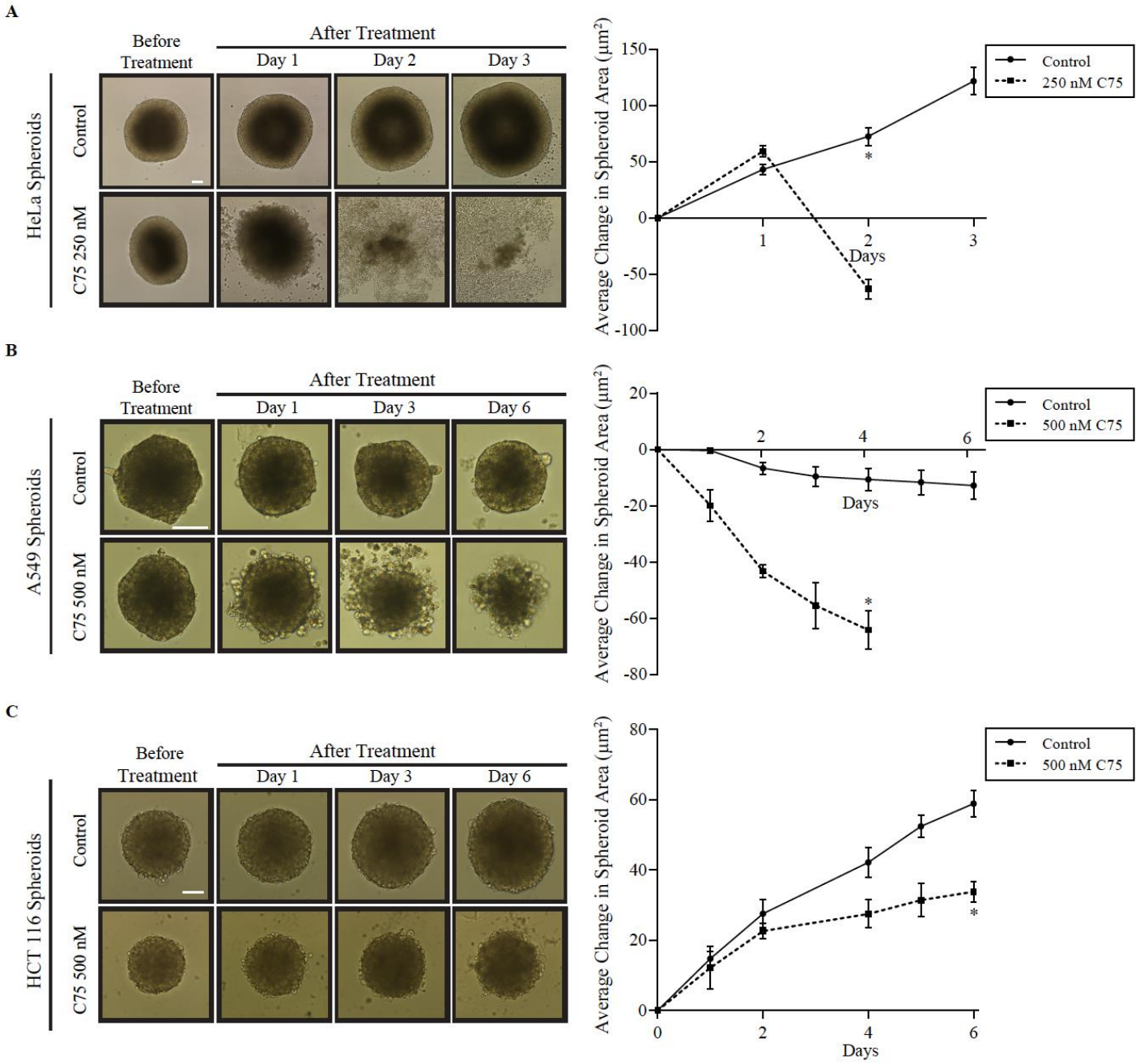
A
Before Treatment
After Treatment
Day 1
Day 2
Day 3
HeLa Spheroids
Control
C75 250 nM
Average Change in Spheroid Area (μm²)
150
100
50
0
-50
-100
1
2
3
Days
*
Control
250 nM C75
B
Before Treatment
After Treatment
Day 1
Day 3
Day 6
A549 Spheroids
Control
C75 500 nM
Average Change in Spheroid Area (μm²)
20
0
-20
-40
-60
-80
2
4
6
Days
*
Control
500 nM C75
C
Before Treatment
After Treatment
Day 1
Day 3
Day 6
HCT 116 Spheroids
Control
C75 500 nM
Average Change in Spheroid Area (μm²)
80
60
40
20
0
0
2
4
6
Days
*
Control
500 nM C75

Figure 11: Nanoparticle delivery improves C75 efficacy in HeLa and A549 spheroids. A) Brightfield images show HeLa spheroids over 3 days before and after treatment with empty NPs (control) or 250 nM of encapsulated C75 (n=5 for each treatment). A line graph shows the change in spheroid area (μm^2) as indicated. B) Images and a graph of A549 spheroids are shown as in A), except that 500 nM of encapsulated C75 (n=5 for each treatment) was used and spheroids were monitored over 6 days. C) Images and a graph of HCT 116 spheroids are shown as in B) (n=3 for each treatment). The scale bar for all images is 0.1 mm. Bars on the graphs show standard deviation, and the asterisks indicate $p<0.05$ determined by the student t test.

3.6 Paclitaxel enhances C75 phenotypes

We also wanted to determine if C75 has the potential to be used in combination therapies. Paclitaxel is a spindle inhibitor that disrupts microtubule dynamics and is used to treat a plethora of cancers. However, it can cause severe side-effects, and patients often develop resistance. Thus, it is ideal to find other drugs that could enhance its effects for use at lower concentrations. First, we assessed the effect of combining paclitaxel and C75 at the cellular level. HCT 116 cells treated with paclitaxel, C75 or both for 7 hours were fixed and co-stained for chromatin (DAPI; blue) and microtubules (green). Paclitaxel caused a significant increase in the proportion of HCT 116 cells with monopolar, bipolar misaligned and/or multipolar/fragmented spindle phenotypes (Fig. 12). The majority of phenotypes did not significantly change between 2.5 – 100 nM of paclitaxel, however a two-way ANOVA with a post-hoc Tukey's test with 95% confidence intervals indicated that there was a significant increase in the proportion of cells with bipolar misaligned spindles treated with 10 nM paclitaxel, although it is not clear why (Fig. 12A). Increasing the concentration of C75 caused a significant increase in the proportion of cells with spindle phenotypes, which segued from monopolar and bipolar misaligned spindles to the more severe fragmented spindle phenotype. Combining 2.5 nM paclitaxel with C75 appeared to cause an increase in the proportion of cells with fragmented spindles, especially at lower concentrations (Fig. 12A). To quantify this, we calculated a ratio (R) from the observed proportion of cells with fragmented spindles after the combination treatment vs. the predicted proportion determined by adding the treatments together. While $R > 1$ for 2.5 nM paclitaxel with 100 nM C75 (2.17 +/- 0.73), it was close to 1 for 200 (1.45 +/- 0.47) and 300 nM (1.19 +/- 0.2; Fig. 12A). Thus, the multipolar/fragmented phenotype caused by C75 is enhanced by paclitaxel at low concentrations.

We noticed that the spindle poles and/or fragments were clustered closer together in cells treated with paclitaxel compared to C75. This was quantified by measuring the distance between spindle fragments in the different treatments (Fig. 12B). While increasing paclitaxel caused them to move closer together, C75 caused them to move significantly further apart on its own or in combination with paclitaxel (Fig. 12B). This data suggests that C75 also has a different mechanism of action from paclitaxel.

Next, we tested the effects of combining C75 and paclitaxel on spheroid growth. As shown above, we found that 500 nM of C75 prevented HCT 116 spheroids from growing, while 1 uM

caused regression (Fig. 6). However, encapsulation of C75 did not increase its efficacy in HCT 116 spheroids (Fig. 11). Thus, we determined if combining C75 with paclitaxel could have a greater impact on HCT 116 spheroids. While 250 nM C75 or 10 nM paclitaxel prevented the growth of spheroids compared to control (DMSO), adding C75 and paclitaxel together caused spheroids to regress (Fig. 13). Thus, a potential application for C75 could be in combination therapies with paclitaxel, to lower the dose required to effectively treat cancers.

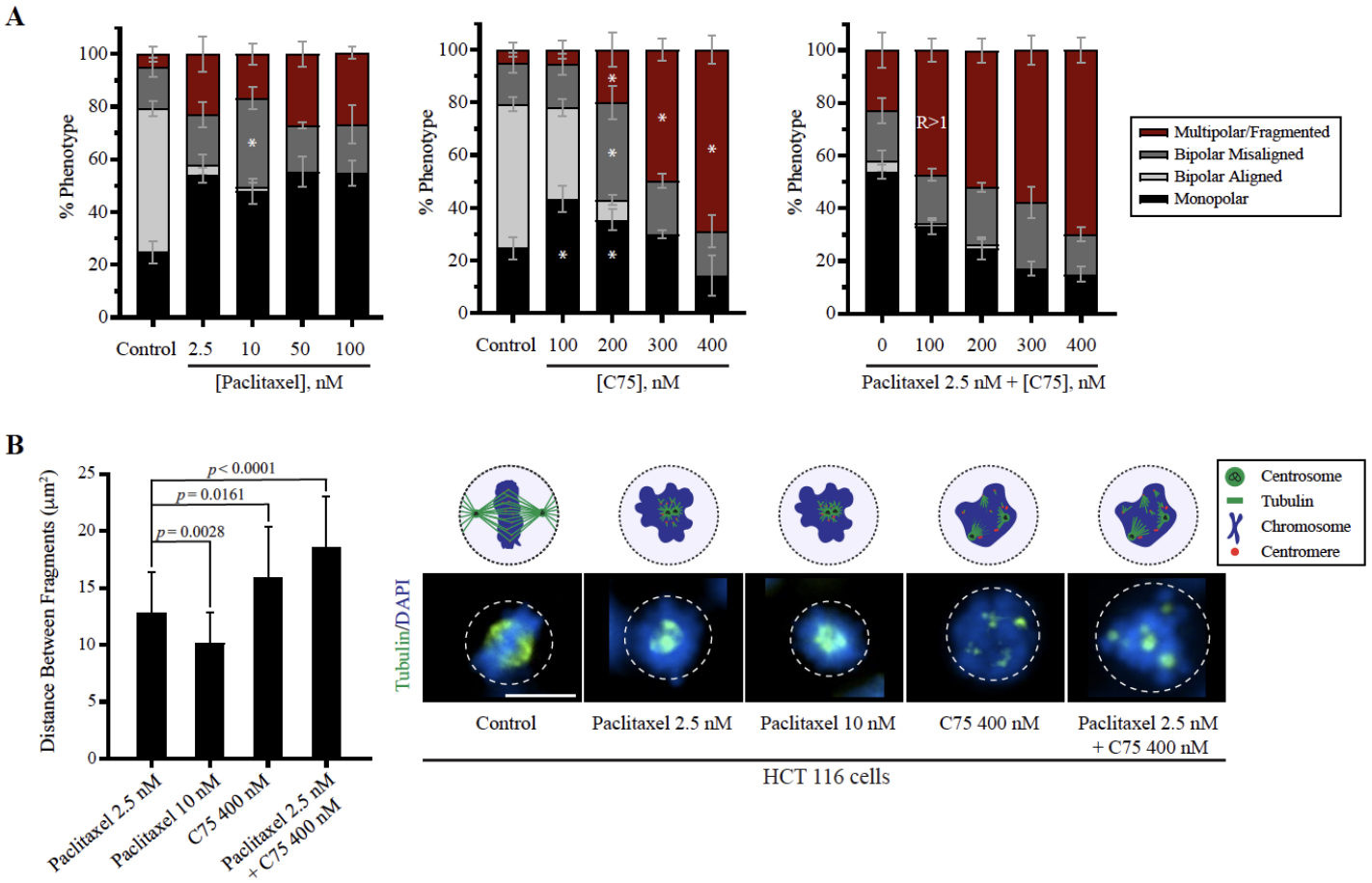

Figure 12: Paclitaxel enhances C75 phenotypes in cells. A) Bar graphs show the proportion of HCT 116 cells with bipolar aligned (light grey), bipolar misaligned (dark grey), multipolar/ fragmented (dark red) or monopolar (black) spindles 7 hours after treatment with C75, paclitaxel or both (n=100 for each treatment). B) A bar graph shows the distance between spindle pole fragments measured for the cells in A) (n=5 for each treatment). Immunofluorescence images show cells co-stained for DAPI (chromatin; blue) and tubulin (green). Phenotypes are shown in the cartoons above. The scale bar is 10 μm. All experiments were done in triplicates. Statistical analyses in A) were done by Dilan Jaunky.

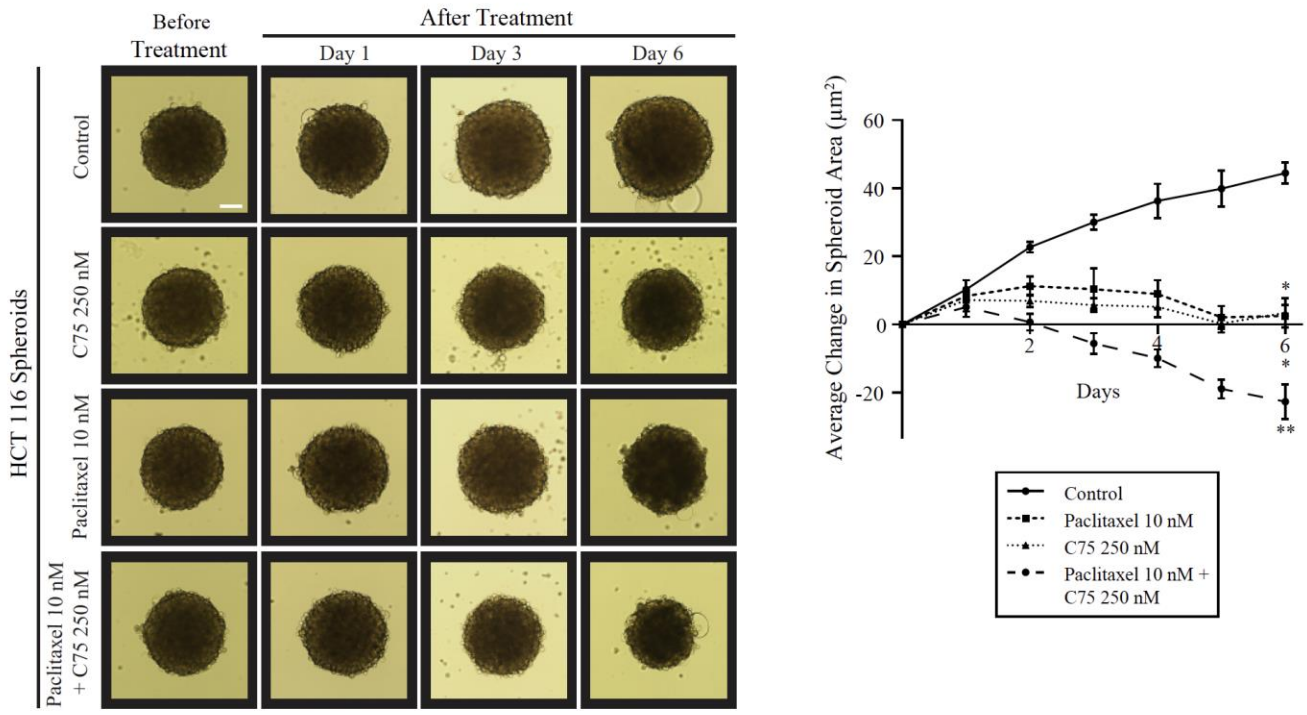

Figure 13: Paclitaxel enhances C75 phenotypes in spheroids. Brightfield images show HCT 116 spheroids over 6 days after treatment with control (DMSO), C75 or paclitaxel or both (n=5 for each treatment). The scale bar is 0.1 mm. A line graph shows the change in spheroid area (μm^2) over time. Bars for all graphs show standard deviation. The asterisks are $p<0.05$ determined by the student t test.

Discussion

We show that a novel anti-cancer compound, C75, selectively arrests cancer cells in mitosis and disrupts or reduces spheroid growth. This compound is a thienoisoquinoline derivative that was synthesized by Dr. Forgione's group. These compounds share a core scaffold with multiple functional groups amenable to modification for structure-activity-relationship studies (SAR) (Beccalli et al., 2008; Wong and Forgione, 2012; Chen et al., 2014). They were designed to have properties ideal for *in vivo* use, and to probe molecular space common to structures found in protein folds and nucleic acids. The phenotypes caused by C75 are unique to this derivative and are not due to the scaffold, since C87, which lacks some of the critical functional groups found in C75, has no effect on cell viability or spheroid growth. C75 disrupts or regresses spheroids grown from HeLa, A549 and HCT 116 cells in the nanomolar range. In addition, its encapsulation in a novel polymeric NP with dual controlled release designed by Dr. Oh's group (Chemistry, Concordia University) increased its efficacy >2-fold in HeLa and A549 spheroids. Importantly, C75 appears to have a different mechanism of action compared to paclitaxel and we found that it had a greater impact on cells and spheroids when used in combination with paclitaxel.

The ability of C75 to reduce spheroids grown from multiple cancer cell lines highlights its potential for *in vivo* use. Our previous studies showed that C75 reduces cancer cell viability in the nanomolar range by causing mitotic arrest due to disruption of the bipolar spindle. However, these studies were done using cells grown in a dish as a monolayer (2D), which may not necessarily reflect how a drug would work in a tumour microenvironment. Multi-cellular tumour spheroids grown from cultured cells more accurately reflect drug efficacy *in vivo*, although they do not fully replace *in vivo* experiments since they lack a bloody supply and other cell types. Excitingly, C75 on its own or encapsulated in biodegradable NPs completely disrupted or reduced spheroids grown from HeLa, A549 and HCT 116 cells in the nanomolar range. This data suggests that C75 has the potential to work on tumours *in vivo* and merits further studies in animal models. Interestingly, C75 had higher efficacy in HeLa spheroids (complete disruption at 500 nM) in comparison to A549 (regression) or HCT 116 (slowed growth) spheroids. Spheroids grown from the different cell lines differ both genetically and physically. For example, HeLa spheroids are less packed and resemble a flat disc vs. a sphere, which could make a greater number of cells more accessible to C75. A549 and HCT 116 spheroids are more tightly packed, which could restrict access of the

drug to cells that are more interior. Genetic changes also could reduce the efficacy of C75 depending on what genes are up and/or down-regulated. For example, upregulation of MDR1 could pump C75 out of cells causing it to be less effective (Oshikata et al., 2011). Other changes could alter the molecular target of C75 causing it to have lower affinity and/or less accessible.

The increased efficacy of C75 in HeLa and A549 spheroids using NPs provides a proof-of-concept that warrants making different modifications that could improve its selectivity and efficacy *in vivo*. However, C75 did not have increased efficacy in HCT 116 spheroids. This could reflect differences in gene expression that occur upon formation of HCT 116 spheroids, which make these cells more resistant to NP uptake and/or their ability to release C75. Thus, modifications for improving C75 for use in colorectal cancers may need to be different vs. those for other cancers. Adding moieties such as peptides that could bind to specific receptors that are over-expressed on the surface of a subset of cancers could target the compound more selectively to these cancers and reduce side-effects. Alternatively, adding a large molecular weight moiety that already is known to be safe, such as albumin could improve the retention of C75 in the bloodstream in a non-selective way.

C75 appears to have a different mechanism of action compared to paclitaxel, suggesting that it could be explored for use in combination therapies (Dumontet and Jordan, 2010). Although both C75 and paclitaxel cause mitotic spindle defects, the spindle phenotypes differ. For example, while paclitaxel treatment increased the proportion of HCT 116 cells with monopolar spindles (centrosomes/spindle poles fail to separate), C75 caused an increase in the proportion of cells with multipolar/fragmented spindles and combining the drugs enhanced the fragmentation phenotype. Many cancer cells have an increase in the number of centrosomes (*e.g.* due to amplification or failed division) or aberrant centrosomes prone to fragmentation of the PCM (Maiato and Logarinho, 2014). While this phenotype should lead to the formation of multipolar spindles and death due to extreme aneuploidy, cancer cells have adapted mechanisms that cluster centrosomes or fragments to form bipolar spindles. Thus, finding compounds that target this machinery should improve their selectivity for cancer vs. healthy cells. HCT 116 cells already have a high proportion of monopolar spindles compared to other cell lines. They have over-expressed ch-TOG, a microtubule polymerase that decreases microtubule dynamics and stabilizes microtubules (Barr and Gergely, 2008). This may make it harder for centrosomes to separate and adding paclitaxel, which also stabilizes microtubules, increases this phenotype even more. While we do not know

the molecular target of C75, our data shows that it disrupts spindle poles and causes fragmentation, which clearly over-rides the increase in microtubule stabilization in HCT 116 cells. To help us identify a potential biomarker, we need to compare the RNA and protein expression profiles of our most responsive cell lines to find changes they have in common. For example, HCT 116 cells have over-expressed ch-TOG, but it is not clear if it is similarly over-expressed in the other cell lines. There could be other genetic changes that arose in conjunction with ch-TOG, and one of these proteins also could be the target of C75. Regardless, we favour the hypothesis that C75 targets a regulator of the PCM that is more strongly required in cancer cells. In support of C75 and paclitaxel having distinct mechanisms of action, they more strongly reduced HCT 116 spheroid growth when added together at subthreshold concentrations vs. each on their own. Thus, this data supports further investigating the use of C75 in combination therapies with other anti-cancer drugs.

Our next step is to test C75 in an animal model to determine its safety, bioavailability and efficacy *in vivo*. For example, we will determine the maximal tolerated dose by an organism. To do this, we inject mice with C75 subcutaneously at varying concentrations and measure changes in their weight. Lethargy and weight loss are signs that the drug has a negative impact on their overall physiology. The blood also will be tested for C75 bioavailability and for metabolic reactivity to determine how often the drug needs to be administered. Once an ideal dosage and schedule for administration is established, we will test the ability of C75 to disrupt and/or reduce the growth of xenografts in mice derived from the same cell lines that our drug is most responsive to (*e.g.* A549 and HCT 116 cells). A subsequent goal would be to test for the potential for C75 to be administrated orally, and for its ability to successfully treat patient-derived xenografts.

References

Akhmanova, A., and Steinmetz, M.O. (2015). Control of microtubule organization and dynamics: two ends in the limelight. Nat. Rev. *Mol. Cell Biol*. 16: 711-726.

Barr, A. and Gergely, F. (2008). MCAK-Independent Functions of ch-Tog/XMAP215 in Microtubule Plus-End Dynamics. *Mol. Cell. Biol*. 28(23):7199-7211.

Beccalli, E.M. Broggini, G. Martinelli, M., and Sottocornola, S. (2008). Microwave-assisted intramolecular cyclization of electron-rich heterocycle derivatives by a palladium-catalyzed coupling reaction. *Synthesis.* 1: 136-140.

Burgess, S. G., Peset, I., Joseph, N., Cavassa, T., Vernos, I., Pfuhl, M., Gergely, F., and Bayliss, R. (2015). Aurora-A-Dependent Control of TACC3 Influences the Rate of Mitotic Spindle Assembly. *PLoS Genet*. 11(7): 1-36.

Cao, YN., Zheng, LL., Wang, D., Liang, XX., Gao, F. and Zhou, XL. (2017). Recent advances in microtubule-stabilizing agents. *Euro. J. Med. Chem*. 143: 806-828.

Changenet-Barret, P., Gustavsson, T., Markovitsi, D., Manet, I. and Monti, S. (2013). Unravelling molecular mechanisms in the fluorescence spectra of doxorubicin in aqueous solution by femtosecond fluorescence spectroscopy. *Phys. Chem*. 15: 2937-2944.

Chen, F. Wong, N.W.Y., and Forgione, P. (2014). One-pot tandem palladium-catalyzed decarboxylative cross-coupling and C-H activation route to thienoisoquinolines. *Adv. Synth. Cat.* 365: 1725-1730.

Cui, X., Hartanto, Y., and Zhang, H. (2017). Advances in multicellular spheroids formation. J R SOC Interface. 14(127).

Dumontet, C. and Jordan, MA. (2010). Microtubule-binding agents: a dynamic field of cancer therapeutics. *Nat Rev Drug Discov*. 9(10): 790-803.

Fielding, A.B., Lim, S., Montgomery, K., Dobreva, I., and Dedhar, S. (2010). A critical role of integrin-linked kinase, ch-TOG and TACC3 in centrosome clustering in cancer cells. *Oncogene*. 30: 521-534.

Fox, C. J., Howard, A. E., Currie, D. J., Rogers, L. S. and Slep, C. K. (2014). The XMAP215 family drives microtubule polymerization using a structurally diverse TOG array. *Mol. Biol. Cell*. 25(16): 2375-2392.

Friedrich, J., Seidel, C., Ebner, R. and Kunz-Schughart, A. L. (2009). Spheroid-based drug screen: considerations and practical approach. *Nat. Protoc*. 4(3): 309-324.

Ghosh,S., Spagnoli, C.G., Martin, I., Ploegert, S., Demougin, P., Heberer, M. and Reschne, A. (2005). Three-dimensional culture of melanoma cells profoundly affects gene expression profile: A high density oligonucleotide array study. *J. Cell. Phys*. 204(2): 522-531.

Hanahan, D., and Weinberg, R.A. (2011). Hallmarks of cancer: the next generation. *Cell.* 144: 646-674.

Hannigan, G. E., Leung-Hagesteijn, C., Fitz-Gibbon, L., Coppolino, M. G., Radeva, G., Filmus, J., Bell, C. J., and Dedhar, S. (1995). Regulation of cell adhesion and anchorage-dependent growth by a new beta 1-integrin-linked protein kinase. *Nature*. 379(6560): 91-96

Hay, M., Thomas D.W., Craighead J.L., Economides C., and Rosenthal, J. (2014). Clinical development success rates for investigational drugs. *Nature Biotech*. 32: 40-51.

Hirschhaeuser, F., Menne, H., Dittfield, C., West, J., Mueller-Klieser, W., and Kunz-Schughart, L.A. (2010). Multicellular tumor spheroids: an underestimated tool is catching up again. *J. Biotechnol.* 148: 3-15.

Indovina, P., Rainaldi, G., and Santini, M. T. (2008). Hypoxia Increases Adhesion and Spreading of MG-63 Three-dimensional Tumor Spheroids. *Anticancer Res*. 28: 1013-1022.

Kalra, J., Warburton, C., Fang, K., Edwards, L., Daynard, T., Waterhouse, D., Dragowska, W., Sutherland, B. W., Dedhar, S., Gelmon, K., and Bally, M. (2009). QLT0267, a small molecule inhibitor targeting integrin-linked kinase (ILK), and docetaxel can combine to produce synergistic interactions linked to enhanced cytotoxicity, reductions in P-AKT levels, altered F-actin architecture and improved treatment outcomes in an orthotopic breast cancer model. *Breast Cancer Research*. 11(3): 1465-1542.

Levine, MS., Bakker, B., Boeckx, B., Moyett, J., Lu, J., Vitre, B., Spierings, DC., Lansdorp, PM., Cleveland, DW., Lambrechts, D., Foijer, F. and Holland, AJ. (2017). Centrosome amplification is sufficient to promote spontaneous tumorigenesis in mammals. *Dev Cell*. 40(3): 313-322.

Lorenzo, A. C. and Concheiro, A. (2014). Smart drug delivery systems: from fundamentals to the clinic. *Chem. Commun*. 50(58): 7743-7765.

Lüders, J. and Stearns, T. (2007). Microtubule-organizing centres: a re-evaluation. *Nature Reviews.* 8: 161-167.

Maiato, H., and Logarinho, E. (2014). Mitotic spindle multipolarity without centrosome amplification. *Nature Cell Biology*. 16: 386-394.

McGowan, J., Chung, R., Maulik, A., Piotrwska, I., Walker, J.M. and Yellon, D.M. (2017). Anthracycline Chemotherapy and Cardiotoxicity. *Cardiovasc Drugs Ther*. 31(1): 63-75.

Oshikata, A., Matsushita, T., and Ueoka, R. (2011). Enhancement of drug efflux activity via MDR1 protein by spheroid culture of human hepatic cancer cells. *J of Bioscience and Bioengineer*. 111(5). 590-593.

Qin, J., and Wu, C. (2012). ILK: a pseudokinase in the center stage of cell-matrix adhesion and signaling. *Curr Opin Cell Biol*. 24(5): 607-613.

Quintyne, N. J., Reing, E. J., Hoffelder, R. D., Gollin, M. S. and Saunders, S. W. (2005). Spindle Multipolarity Is Prevented by Centrosomal Clustering. *Science*. 307(5706): 127-129.

Pannu, V., Rida. P. C. G., Ogden, A., Turaga, R. C., Donthamsetty, S., Bowen, N. J., Rudd, K., Gupta, M. V., Reid, M. D., Cantuaria, G., Walczak, C. E., and Aneja, R. (2015). HSET

overexpression fuels tumor progression via centrosome clustering-independent mechanisms in breast cancer patients. *Oncotarget*. 2015;6(8):6076-6091.

Patel, N.R., Aryasomayajula, B., Abouzeid, A.H., and Torchilin, V.P. (2015). Cancer cell spheroids for screening of chemotherapeutics and drug-delivery systems. *Ther. Deliv*. 6: 509-520.

Phung, T. Y., Barbone, D., Broaddus, V. C. and Ho, M. (2011). Rapid Generation of *In Vitro* Multicellular Spheroids for the Study of Monoclonal Antibody Therapy. *J Cancer*. 2: 507-514.

Stadler, M. et al. (2015). Increased complexity in carcinomas: Analyzing and modeling the interaction of human cancer cells with their microenvironment. Semin. *Cancer Biol*. 35: 107-124.

Sutherland, M. R. (1988). Cell and Environment Interactions in Tumor Microregions: The Multicell Spheroid Model. *Science*. 240: 177-184.

Trachootham, D., Alexandre, J. and Huang, P. (2009). Targeting cancer cells by ROS-mediated mechanisms: a radical therapeutic approach? *Nat. Rev. Drug Disc*. 8: 579-591.

Tilney, G.L., Bryan, J., Bush, J. D., Fujiwara, K., Mooseker, S. M., Murphy, D. B. and Snyder, D. H. (1973). Microtubules: Evidence for 13 protofilaments. *J Cell. Biol*. 59(2): 267-275.

Van der Ende, E. A., Kravitz, J. E. and Harth, E. (2008). Approach to Formation of Multifunctional Polyester Particles in Controlled Nanoscopic Dimensions. *J. AM. CHEM. SOC*. 130: 8706-8713.

Watts, C. A., Richards, F. M., Bender, A., Bond, P. J., Korb, O., Kern, O., Riddick, M., Owen, P., Myers. R. M., Raff, J., Gergely, F., Jodrell, D. I., and Ley, S. V. (2013). Design, Synthesis, and Biological Evaluation of an Allosteric Inhibitor of HSET that Targets Cancer Cells with Supernumerary Centrosomes. *Chemistry & Biology*, 20(11), 1399–1410.

Wong, N.W.Y, and Forgione, P. (2012). A one-pot double C–H activation palladium-catalyzed route to a unique class of highly functionalized thienoisoquinolines. *Org. Lett*. 14: 2738-2741.

Yun, B. W., Yan, Z., Amir, R., Hong, S., Jin, Y. W., Lee K. E., and Loake, G. J. (2012). Plant natural products: history, limitations and the potential of cambial meristematic cells. *Biotechnology and Genetic Engineering Reviews*. 28(1), 47-60